Creep and shrinkage of nonproprietary ultra-high-performance concrete

Garrett Tatum, Lautaro Martinez, and Natassia Brenkus

- Four nonproprietary ultra-high-performance concrete (UHPC) mixture designs were developed by precasters in North America to study creep and shrinkage effects. The UHPC specimens were cured under either ambient or steam conditions.
- Accepted test procedures were applied to characterize long-term material behavior. Testing modifications were made to address properties unique to UHPC, such as presence of fibers, high compressive strengths, and the development of a rough surface that forms before the initial set of the material.
- The study reviewed how the long-term creep and shrinkage behavior of UHPC differs from the design estimations used for conventional concrete.

Development and use of ultra-high-performance concrete (UHPC) has gained momentum in recent years, particularly in overlays, repairs, and other applications.[1–3] Members of the precast concrete industry and public transportation agencies have made numerous efforts to develop designs for nonproprietary UHPC mixture proportions.[4–9] The precast concrete industry recently undertook a large experimental effort to develop nonproprietary UHPC for use in large-scale production by precasters; the investigation involved extensive testing to design mixture proportions, novel sections, and recommended mechanical properties.[10] The work discussed in this article provides supplementary data on creep and shrinkage performance in support of that recent project.

UHPC mixtures are composed of a variety of raw materials, steel fibers, supplementary cementitious materials, and other additives. In comparison with conventional concrete mixture proportions, UHPC mixture proportions are denser and have improved mechanical behavior and durability. Several publications have described UHPC tensile behavior,[10–15] flexural behavior,[11,12] compressive behavior,[16-18] and durability.[19–21]

Creep and shrinkage properties of UHPC have received little attention.[10,11,22,23] This omission is significant because inaccurate estimation of creep and shrinkage in prestressed components—the primary contributors to prestress loss—can lead to unexpected deformations, including excessive camber, deflection, and cracking.[24] This article offers a novel contribution by advancing understanding of creep

and shrinkage behavior of nonproprietary UHPC mixtures for large-scale precast concrete construction, as well as the influence of accelerated curing on these behaviors.

Creep and shrinkage are influenced by several interrelated factors, including curing conditions, mixture proportions, and environmental conditions. In the case of prestressed concrete components, the prestress magnitude, concrete age at prestressing, and location of the applied prestress force with respect to the cross section may also influence creep. For convenience, creep and shrinkage are often considered separately, although they are interdependent aspects of complex physical phenomena.[24] These phenomena have been extensively studied and characterized for conventional concrete materials. As a result, the behavior of conventional concrete under these effects is comprehensively understood, and this understanding has been applied to develop reliable estimation approaches, which have been adopted in design guidelines used widely within the industry.

The development of similar design guidelines for UHPC requires both new research and reassessment of established creep and shrinkage estimation approaches, which may not be appropriate for the distinctive behavior of UHPC mixture proportions or UHPC production methods. Characterization of creep and shrinkage as primary contributors to prestress loss is critical as the industry moves toward the adoption of UHPC structural components. This work aimed to provide creep and shrinkage data for nonproprietary UHPC mixture proportions explicitly developed for use in the precast concrete industry.

To characterize creep and shrinkage of UHPC, the experimental study of creep and shrinkage properties described in this article was performed on nonproprietary UHPC mixture proportions developed by the PCI-UHPC project in conjunction with several precasters across the United States and Canada.[10] This research generated the first data on the creep and shrinkage properties of these UHPC mixture proportions. This research used several ASTM International test methodologies to investigate creep and shrinkage behavior with modifications made to accommodate several properties of UHPC, including, most notably, the presence of fibers, high compressive strengths, and the development of a rough surface of limited depth that forms before the initial set of the material, referred to as "elephant skin" (**Fig. 1**). The efforts to adopt ASTMs related to the unique properties of UHPC involved several challenges; these challenges are discussed herein to contribute "lessons learned" for future characterization efforts.

Experimental program

Materials

Four nonproprietary, precaster-developed UHPC mixture proportions were used to evaluate creep and shrinkage phenomena; the participating precasters represented distinct regions in the United States and Canada, including the Pacific Northwest, the Midwest, and the Southeast United States. Each precaster provided their own locally available materials—including cement, sand, supplementary cementitious materials (silica fume, limestone, slag), steel fibers, and chemical additives—to the research team. The PCI-UHPC project report[10] offers more details about these materials, their sources, and the mixture proportion methodology. It should be noted that the steel fibers used in this project largely came from one supplier, reflecting the general supply chain of steel fibers in the United States. The chemical admixtures were selected based on the precasters' preferred suppliers. The experimental study referred to these mixture proportions as mixture 1, mixture 2, mixture 3 and mixture 4. The specimens were labeled 1, 2, 3, or 4 for each of the mixture proportions followed by either a letter A or S, which refer to ambient and steam curing conditions, respectively. Owing to laboratory closures related to the COVID-19 pandemic, the test matrix does not include all combinations of mixture proportions and curing conditions.

Samples

Each batch was mixed per the precaster's instructions using an 80-L Skako orbital pan mixer. The volume of water was adjusted to consider the sand moisture content measured in accordance with ASTM C566, *Standard Test Method for Total Evaporable Moisture Content of Aggregate by Drying*.[25] The general batching procedure was similar for all concrete mixtures with slight variations in the order in which mixture components were added and the volume of water added. Sand and silica fume were added to the mixer before the mixer was started, and then mixed thoroughly. Cement was then added to the mixer while it was running. Ice water and admixtures were added in accordance with the precaster-specific batching procedure. Mixing continued until the concrete "turned" or became flowable. Steel fibers were added after the mixture turned; this step involved slowly and evenly distributing the fibers through a 1.5 in. (38 mm) steel mesh while the mixer was running. The concrete was mixed for 2 minutes following the completion of fiber addition and then discharged. During batching, the flow was measured in accordance with

Figure 1. Formation of elephant skin on freshly batched ultra-high-performance concrete. Note the surface texture in response to scooping.

ASTM C1437, *Standard Test Method for Flow of Hydraulic Cement Mortar*,[26] as modified by ASTM C1856, *Standard Practice for Fabricating and Testing Specimens of Ultra-High Performance Concrete*;[27] these measurements were taken at the time the mixture turned (before fiber addition) and at the time of batch discharge (after fiber addition).

Curing conditions

Two curing conditions were evaluated: ambient curing and steam curing. Following casting, all specimens were held in laboratory ambient conditions (72°F ± 4.0°F [22.2°C ± 2.2°C] and 40% relative humidity) for 48 hours before unmolding. Specimens were covered with plastic sheets to minimize moisture loss. Specimens were then unmolded and subjected to their specified curing regimen. Ambient-cured specimens were held in laboratory conditions with 72°F ± 4.0°F and 40% relative humidity. Steam-cured specimens were subjected to the conditions of 194°F ± 2.0°F (90°C ± 1.1°C) and 100% relative humidity for 48 hours, as recommended by ASTM C1856,[27] and then allowed to gradually cool to ambient conditions before being stored in laboratory conditions (72°F ± 4.0°F and 40% relative humidity). All specimens were stored in ambient laboratory conditions throughout the remainder of the test protocol.

Shrinkage

Three experimental approaches were used to evaluate the shrinkage phenomenon. ASTM C157, *Standard Test Method for Length Change of Hardened Hydraulic-Cement Mortar and Concrete*,[28] as adapted to conform with ASTM C185627 for use with UHPC, was used to capture both autogenous and total shrinkage strains on prismatic specimens; this method is well known and widely used. Autogenous shrinkage was estimated by immediately wrapping specimens with foil tape after they were unmolded. It should be noted that it is difficult to completely eliminate all drying shrinkage from these types of specimens; therefore, drying shrinkage was probably underestimated slightly. ASTM C157 specifies that initial measurement is to be taken at the time of final setting, as determined by ASTM C191, *Standard Test Methods for Time of Setting of Hydraulic Cement by Vicat Needle*.[29] However, owing to the unique properties of UHPC, including the development of elephant skin, the presence of fibers, and lengthy setting time, the final setting time could not be reliably and consistently determined with this method; this issue has also been reported by others.[30] Therefore, initial measurements were taken at 48 hours after specimen casting.

Shrinkage strains rapidly develop at early ages in UHPC mixtures. Therefore, in the second experimental approach, a supplementary round of prismatic specimens (of the same dimensions as those used for ASTM C157 testing) with embedded GEOKON 4200-L vibrating wire strain gauges were cast to capture autogenous shrinkage effects continuously from the moment of UHPC placement (**Fig. 2**).

Finally, testing in accordance with ASTM C1698,[31] was performed. Because strains that are not due to external forces are most significant in mixtures with low water–cementitious material ratios (such as UHPC), researchers were originally very

Length-change measurements in accordance with ASTM C157

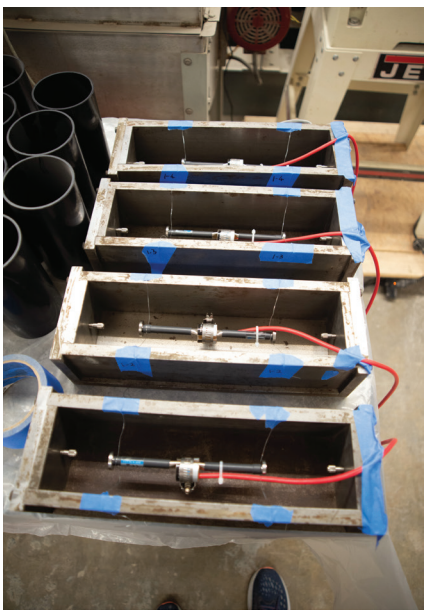

Supplementary specimens for ASTM C157 with embedded strain gauges

Figure 2. Shrinkage test setup

interested in ASTM C1698 testing. For this test method, specimens of freshly mixed UHPC mortar were prepared by placing the material without steel fiber in a standard-specific corrugated mold with sealed ends. Fibers were not used to avoid effects from preferential fiber alignment, as the length of the fibers was similar to the diameter of the molds. The intent of the mold was to provide little resistance to length changes. Again, because the final setting could not be determined, the initial measurements began at 48 hours for all specimens; all other procedures strictly followed the ASTM C1698 guidance.

Despite multiple iterations and refinements to ensure quality control, the ASTM C1698 data were found to be inconsistent and unreliable. Autogenous shrinkage stains are inherently difficult to capture because of the fineness of the developed strains. Instruments with the required resolution were used, but measurements continued to exhibit low precision. As described by ASTM C1698, results are highly dependent on testing conditions and operator work. Although these data are excluded from further consideration herein, the authors do discuss the ASTM C1698 test method to confirm that is difficult to perform.[30]

Creep

To evaluate creep, the study used ASTM C512, *Standard Test Method for Creep of Concrete in Compression*,[32] as modified by ASTM C1856[27] for use with UHPC and with one additional modification to the load magnitude. Whereas the creep testing procedure outlined in the ASTM C512 specifies the maximum applied compressive load as 40% of the tested compressive strength f'_{ci} at time of loading, this research investigated the allowable compressive stress of $0.6f'_{ci}$ from the American Concrete Institute's *Building Code Requirements for Structural Concrete (ACI 318-19) and Commentary (ACI 318R-19)*[33] to better approximate potential creep effects in prestressing applications. The specified initial concrete compressive strength for creep loading was 10 ksi (68.95 MPa). This value was selected to reflect a common compressive strength limit set in prestressing yards at the time of prestress transfer. All specimens were subjected to a compressive stress of 6 ksi (41.4 MPa).

A total of six 3 × 6 in. (76 × 152 mm) cylinders from each batch and curing condition were used. Three specimens were subjected to creep loading and three unloaded companion cylinders were placed in the same room to capture shrinkage effects. To best mimic exposure of the cylinders, the ends of the companion cylinders were taped with foil to prevent moisture loss. All tests were conducted in a controlled-conditioning room maintained at (22.2°C ± 2.2°C) and 50% ± 5% relative humidity.

Three pairs of Whittemore points were mounted within each cylinder mold before casting. A 4 in. (102 mm) nominal gauge length in the longitudinal direction of the cylinders was used and pairs were placed at 120 degree intervals around the cross section. A curing time of 7 days was applied for all the specimens and the compressive strength was verified to be greater than 10 ksi (68.95 MPa) at the time of loading. Squareness was checked with a framing square and feeler gauges to ensure end requirements specified by ASTM C1856. Load was maintained for at least 6 months; in general, large increases in creep strain were not observed after this period.

Results and discussion

Compressive strength and modulus of elasticity

Table 1 summarizes the results obtained for compressive strength and modulus of elasticity (MOE). The data are for both curing regimens (ambient and steam conditions) at 7 and 28 days after casting, and for post-creep loading. The compressive strength for each batch was evaluated according to ASTM C39, *Standard Test Method for Compressive Strength of Cylindrical Concrete Specimens*,[34] as modified for UHPC by

Table 1. Compressive strength and modulus of elasticity of concrete specimens

Specimen	Compressive strength, ksi						Modulus of elasticity, ksi	
	7 days	SD	28 days	SD	Post creep	SD	Ultimate	SD
1-A	19.8	0.2	21.2	1	17.7	1.1	5220	130
2-A	11.3	0.2	19.9*	n/a	17	0.1	3680	19
4-A	15	<0.0	17.8	0.8	19.2	0.8	5210	466
1-S	23.4	<0.0	23.9	0.3	20.2	2.3	5070	130
3-S	19	0.1	20.8	0.4	20.3	0.7	n/a	n/a
4-S	19.9	0.9	19.9	0.3	22.1	0.6	4510	197

Note: SD = standard deviation. n/a=not applicable. 1-A = mixture proportions number 1 with ambient curing conditions; 1-S = mixture proportions number 1 with steam curing conditions; 2-A = mixture proportions number 2 with ambient curing conditions; 3-S = mixture proportions number 3 with steam curing conditions; 4-A = mixture proportions number 4 with ambient curing conditions; 4-S = mixture proportions number 4 with steam curing conditions. 1 ksi = 6.895 MPa.

*Only one cylinder available to test.

ASTM C1856.27 For each batch and curing condition, three specimens were tested at both 7 days and 28 days after casting. The MOE was evaluated for specimens from mixture proportions 1 and 4 in accordance with ASTM C469, *Standard Test Method for Static Modulus of Elasticity and Poisson's Ratio of Concrete in Compression*,[35] as modified for UHPC by ASTM C1856. The test MOE parameters were developed based on the compressive strengths determined in accordance with ASTM C39, with modifications in accordance with ASTM C1856.

As expected, the 28 day compressive strength was greater than the 7-day compressive strength for all specimens. Steam-cured specimens, in general, exhibited greater compressive strengths at 7 and 28 days compared with ambient-cured specimens. Steam-cured specimens had achieved 91% to 100% of their 28-day compressive strength within 7 days; in contrast, ambient-cured specimens exhibited 57% to 93% of their 28-day compressive strength within 7 days. This finding is expected because steam curing increases the cement hydration rate, facilitating a more rapid and complete reaction due to the presence of water and heat. Steam-cured specimens exhibited both greater compressive strengths and MOE, mainly due to accelerated cement hydration. Magnitudes of MOE ranging from 3 to 5 ksi (20.7 to 34.5 MPa) were obtained for ambient-cured specimens, whereas steam-cured specimens exhibited MOE of 4 to 5 ksi (27.6 to 34.5 MPa).

Shrinkage

ASTM C157 testing of autogenous and drying shrinkage For the purposes of analysis, foil-wrapped specimens were assumed to capture the deformations associated with autogenous shrinkage and unwrapped specimens were assumed to capture total shrinkage deformations, including both drying and autogenous effects. Every effort was made to minimize moisture loss from the autogenous shrinkage specimens; however, because of the difficulty of capturing this phenomenon, the value assumed to correspond to autogenous shrinkage likely included some drying shrinkage. Drying shrinkage is defined, for convenience, as the difference between the average recorded strains of the foil-wrapped prisms and the unwrapped prisms. Initial measurements were taken at the time of unmolding, or 48 hours after casting. This time was selected to ensure final set of the mixtures, but it potentially failed to capture early-age autogenous shrinkage. **Figure 3** presents autogenous, total, and drying shrinkage

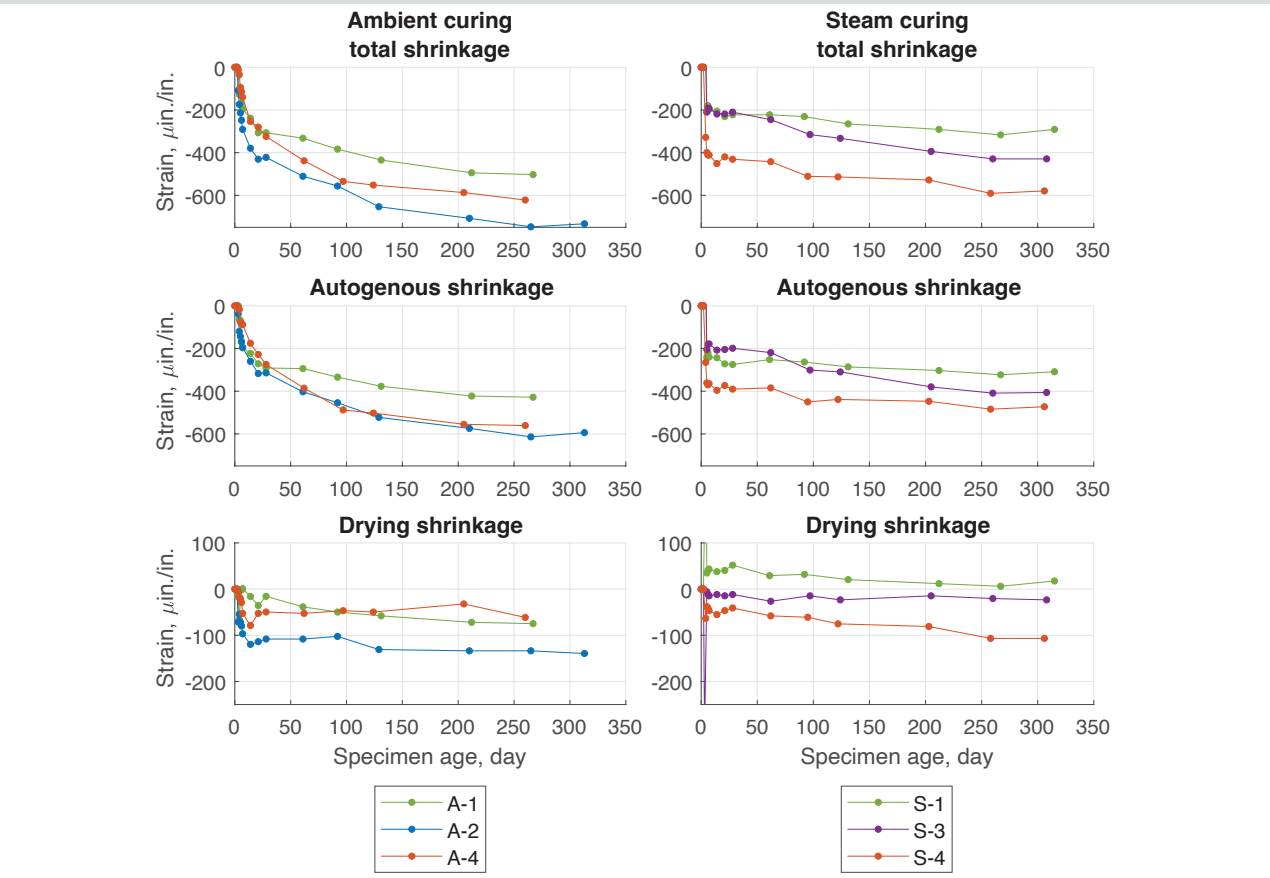

Figure 3. Shrinkage of nonproprietary ultra-high-performance concrete specimens subjected to either ambient or steam curing conditions. Note: 1-A = mixture proportions number 1 with ambient curing conditions; 1-S = mixture proportions number 1 with steam curing conditions; 2-A = mixture proportions number 2 with ambient curing conditions; 3-S = mixture proportions number 3 with steam curing conditions; 4-A = mixture proportions number 4 with ambient curing conditions; 4-S = mixture proportions number 4 with steam curing conditions.

strain for all mixture proportions and curing conditions. **Table 2** summarizes the data corresponding to the final shrinkage values obtained; all data in the table are averaged from three specimens.

The observed total shrinkage varied between approximately 350 to 750 µin./in. Autogenous shrinkage varied from 360 to 690 µin./in. The average total shrinkage was 610 µin./in. for ambient-cured specimens and 433 µin./in. for steam-cured specimens. The average autogenous shrinkage was 526 µin./in. for ambient-cured specimens and 396 µin./in. for steam-cured specimens.

All ambient-cured specimens exhibited greater total and autogenous shrinkage strains than steam-cured specimens. Compared with ambient-curing conditions, steam-curing conditions led to accelerated development of autogenous and total shrinkage at early ages; this finding is consistent with others' findings about the influence of steam curing on shrinkage development.[36] The main reason for this behavior is that the hydration process is accelerated in steam conditions and the pore water self-dries more quickly, causing a sharper development rate of autogenous and total shrinkage (or self-desiccation). Interestingly, the greatest amounts of autogenous, total, and drying shrinkage were observed at early ages (from 3 to 5 days). Other research has illustrated that steam-cured specimens have fewer micropores than ambient-cured specimens and porosity in steam-cured specimens is reduced.[36] Those findings are in part explained by the rapid formation of hydration products through the hydration of silica fume during steam curing and may suggest that negligible shrinkage develops in UHPC components after steam curing is finished. In general terms, the steam-curing regimen reduced the total shrinkage by 28% to 40%.

For the purposes of this research, drying shrinkage was assumed to be the difference between autogenous and total shrinkage. Although it is important to highlight that this assumption neglects the interdependence between drying and autogenous shrinkage, this simplification is widely accepted.[37] Under this consideration, drying shrinkage was observed to be relatively small, with a range of 0 to 140 µin./in. In addition, drying shrinkage was greater in ambient-cured specimens than in steam-cured specimens. In general, the drying shrinkage of most specimens stabilized relatively early in the testing period in the range of 9 to 126 µin./in. The plateau of the drying shrinkage was used to estimate the ultimate drying shrinkage for each specimen, as well as the time that ultimate drying shrinkage was attained.

In contrast to the trend observed in this research for UHPC materials, conventional concrete exhibits more drying shrinkage than autogenous shrinkage.[38] Long-term concrete volume stability (that is, creep and drying shrinkage) is influenced by the water-to-binder ratio (*w*/*b*). The drying shrinkage associated with a *w*/*b* greater than 5 is larger than the drying shrinkage associated with a *w*/*b* in the range of 0.35 to 0.45.[39] UHPC has a low *w*/*b* (around 0.2), and that results in a smaller volume of pore water in the matrix and leads to less drying shrinkage. Because of the addition of fineness admixtures such as silica fume and filler, UHPC has a denser microstructure and a smaller pore size than conventional concrete. Laplace's Law indicates that the capillary pressure from the self-desiccation of pore water is inversely related to the pore radii. Because UHPC has much finer capillary pores than conventional concrete, UHPC has more autogenous shrinkage strains. Based on these two reasons, it is expected that UHPC would exhibit much greater autogenous shrinkage than drying shrinkage.

Prismatic specimens with embedded vibrating wire strain gauges Continuous shrinkage measurements via vibrating wire strain gauges were conducted for 150 days following mixture placement (**Fig. 4**). The initial early-age

Table 2. Final shrinkage

Specimen	Age at final measurement, day	Final shrinkage, µin./in.					
		Total		Autogenous		Drying	
		Mean	SD	Mean	SD	Mean	SD
1-A	315	511	1.1	434	10.9	78	10.9
1-S	315	291	22.3	309	9.2	-2	24.2
2-A	313	733	41	594	13.3	139	43.1
4-A	308	587	13.4	549	5.06	4	14.3
4-S	308	429	13.4	406	13.4	23.4	18.9
4-S	306	579	40.3	473	34.9	107	53.3

Note: SD = standard deviation. 1-A = mixture proportions number 1 with ambient curing conditions; 1-S = mixture proportions number 1 with steam curing conditions; 2-A = mixture proportions number 2 with ambient curing conditions; 4-A = mixture proportions number 4 with ambient curing conditions; 4-S = mixture proportions number 4 with steam curing conditions.

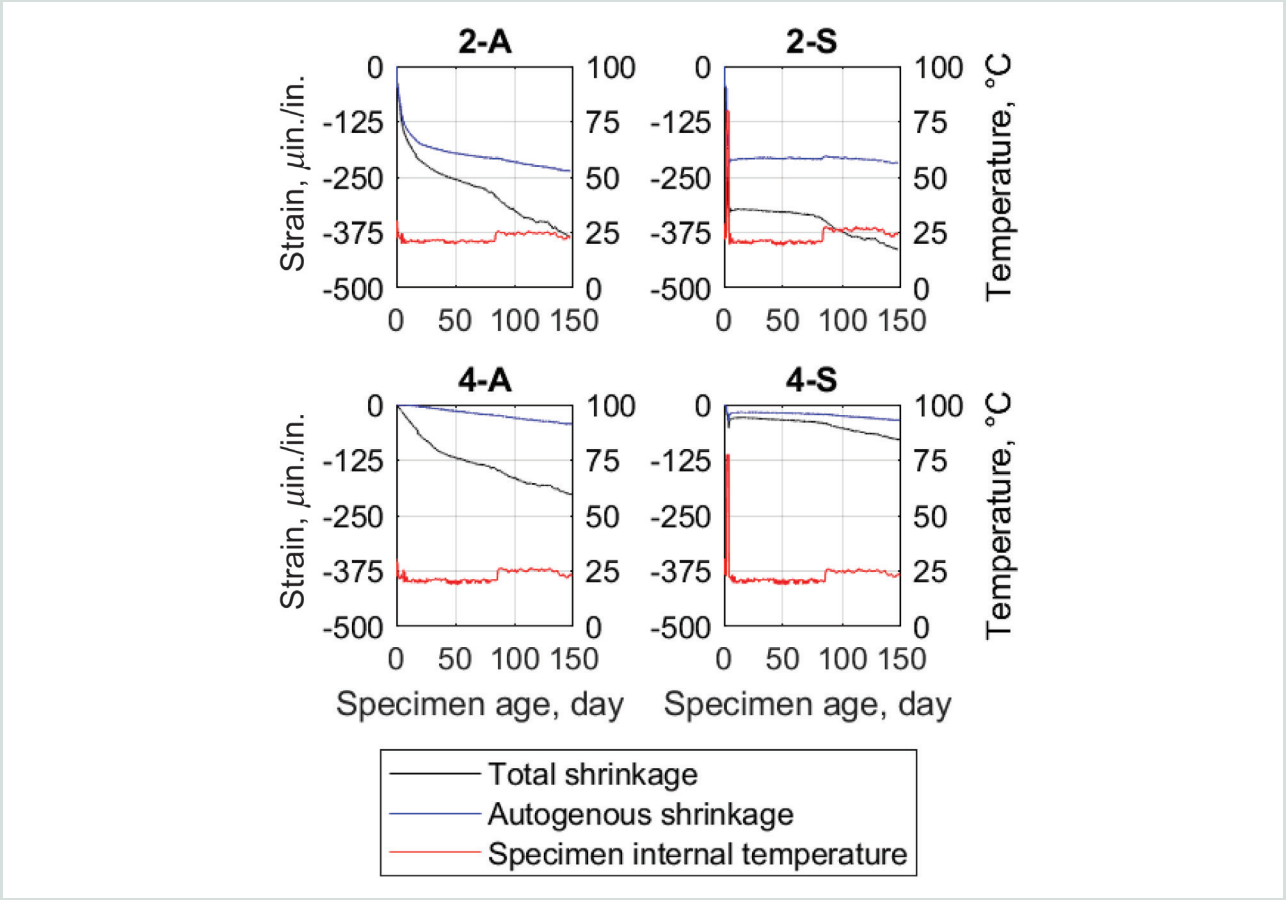

Figure 4. Shrinkage of nonproprietary ultra-high-performance concrete specimens as measured by embedded wire strain gauge. Note: 2-A = mixture proportions number 2 with ambient curing conditions; 2-S = mixture proportions number 2 with steam curing conditions; 4-A = mixture proportions number 4 with ambient curing conditions; 4-S = mixture proportions number 4 with steam curing conditions. °C = (°F – 32)/1.8.

data are shown in **Fig. 5**. These data, unlike other measurements in this report, include the initial 48-hour period (assumed elsewhere as being prior to the final setting time) and span throughout the duration of the steam-curing period (if applicable). **Table 3** shows the final measured values for these specimens.

Autogenous shrinkage seems to be nearly independent of curing condition, but it is unique to each mixture proportion. By the end of the test period, specimens 2-A and 2-S exhibited approximately 220 to 240 μin./in. of autogenous shrinkage, whereas specimens 4-A and 4-S exhibited approximately 40 μin./in.

In contrast, total shrinkage seems to be dependent on the curing condition, suggesting that drying shrinkage is still accumulating. Total shrinkage magnitudes at the end of the test period (150 days) were approximately 414 and 80 μin./in. for the steam-cured specimens 2-S and 4-S, respectively. Ambient-cured specimens 2-A and 4-A exhibited total shrinkage values of approximately 385 and 203 μin./in., respectively. It is interesting to note that specimen 2-A exhibited much greater total shrinkage than its steam-cured counterpart, 2-S, which seems to have stopped accumulating both autogenous and drying shrinkage by the end of the test period.

Steam-cured specimens showed greater shrinkage effects at early ages than ambient-cured specimens (Fig.5, note

Table 3. Shrinkage at 150 days

Specimen	Total shrinkage μin./in.	Autogenous shrinkage μin./in.	Estimated drying shrinkage μin./in.
2-A	385	237	148
2-S	414	218	196
4-A	203	44	159
4-S	80	35	45

Note: 2-A = mixture proportions number 2 with ambient curing conditions; 2-S = mixture proportions number 2 with steam curing conditions; 4-A = mixture proportions number 4 with ambient curing conditions; 4-S = mixture proportions number 4 with steam curing conditions.

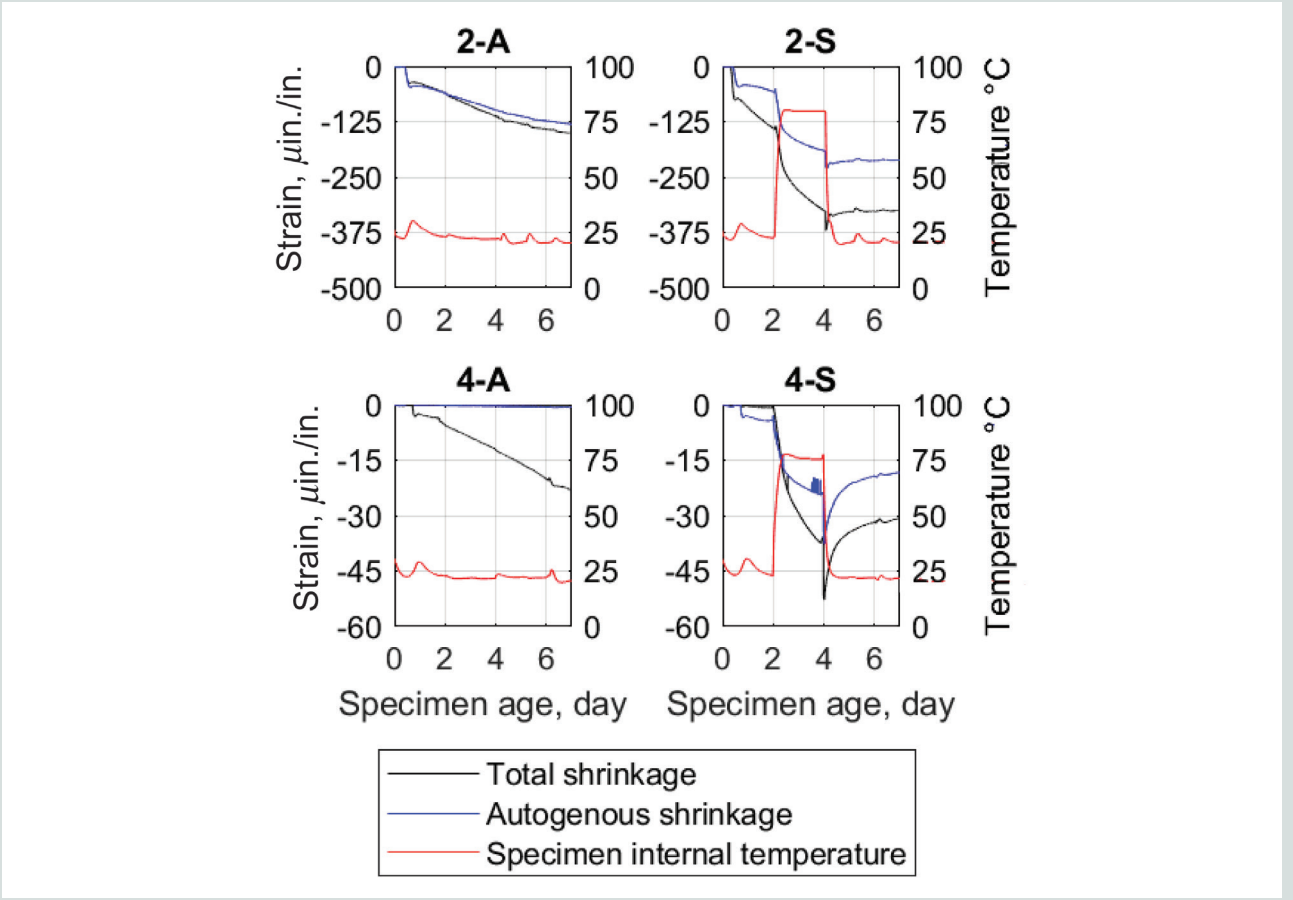

Figure 5. Early-age shrinkage of nonproprietary ultra-high-performance concrete specimens. Note: 2-A = mixture proportions number 2 with ambient curing conditions; 2-S = mixture proportions number 2 with steam curing conditions; 4-A = mixture proportions number 4 with ambient curing conditions; 4-S = mixture proportions number 4 with steam curing conditions. °C = (°F – 32)/1.8.

that the y-axis scales are different for each mixture). This finding is expected, but, interestingly, steam-curing treatment significantly affects the strain development. In the two tested mixture proportions (which otherwise exhibited very different shrinkage development profiles), most of the strain increase was observed while the samples were in steam curing conditions (2 to 4 days), providing evidence of the rapid increase in the cement hydration rate. Following the steam-curing protocol, very little shrinkage strain occurred. This effect would have been unobservable if shrinkage were only assessed by ASTM C157.[28] ASTM C157 testing data may therefore incorrectly suggest that little to no shrinkage is developing in steam-cured UHPC, when, in reality, most shrinkage is simply occurring before strain measurements begin. Depending on the production method used to cast a UHPC component and the curing regimen applied, this error could have important implications for determining prestress losses.

ASTM C1698 Evaluation of autogenous shrinkage

Autogenous shrinkage was assessed following the specifications of ASTM C1698.[31] Three separate efforts were done to produce test specimens. The specimen environment and the methodology for data collection were highly controlled during the tests. Nevertheless, the data show high variability and inconsistencies. The authors have chosen to comment on the challenges encountered for future research about the potential problems and difficulties in measuring autogenous shrinkage of UHPC materials with ASTM C1698.

Three replicate specimens without fibers were tested for each material batch and curing condition. Despite the efforts made to reduce the sources of error in the test, some variability in the measurements was observed. This variability may be associated with specific characteristics of the test setup and the casting of the specimens that cannot be controlled. These issues have been noted by previous researchers.[40]

The measurement of the autogenous shrinkage should start when the cement matrix has developed a solid composition and begins to transfer tensile stress.[41] However, there may be potential measurement problems associated with the setup, instrumentation, and preparation of the specimens. Additionally, researchers must correctly define the "time zero" (the time for starting the shrinkage measurements). The proper selection of the starting point is essential for a correct interpretation of the results because it determines the baseline for future measurements.

ASTM C1698 defines that the first measurement should be taken at the final setting time determined by the use of Vicat apparatus. In this test, the final set time (time zero for ASTM C1698) is described as the moment when the device needle does not penetrate the material surface when dropped upon it. This is a qualitative indication and is dependent on the judgment of the researcher conducting the test. In addition, in some specimens, penetration marks were exhibited even 48 hours after casting, potentially due to the formation of elephant skin on test specimens.

Other authors have provided alternate methodologies to define the time zero for measuring autogenous shrinkage strains of UHPC. For example, Graybeal defined final set time as "a penetration resistance of 27.60 MPa (4 ksi) at about 18–20 h after casting" based on the 2000 edition of AASHTO T197, *Standard Method of Test for Time of Setting of Concrete mixtures by Penetration Resistance*.[11,42,43] However, there is still no agreement about what time should be defined as time zero to begin the measurement of the shrinkage.

Creep

Creep specimens were monitored for a period of approximately 12 to 18 months. At the end of the test period, creep strains of approximately 1000 to 1500 µin./in. were observed in ambient-cured specimens; steam-cured specimens exhibited creep strains of 300 to 600 µin./in. (**Fig. 6**). Most of the creep strain was observed to develop during the first 100 days of loading. The last data point on the plots shown in Fig. 6, represents the strain following the unloading. This value was used to roughly verify that the creep frames remained under the expected load through the test duration. All test specimens except ambient-cured mixture proportion 4 exhibited net negative creep strain; that means the recovered elastic strains were greater in magnitude than the creep strain, a finding that is expected in UHPC materials because of their high MOE.[32]

Creep coefficient The creep coefficient is defined as the ratio of the final creep strain under loading to the initial elastic strain (**Fig. 7**). Creep coefficient values of approximately 0.20 to 1.20 were observed in the ambient-cured specimens.

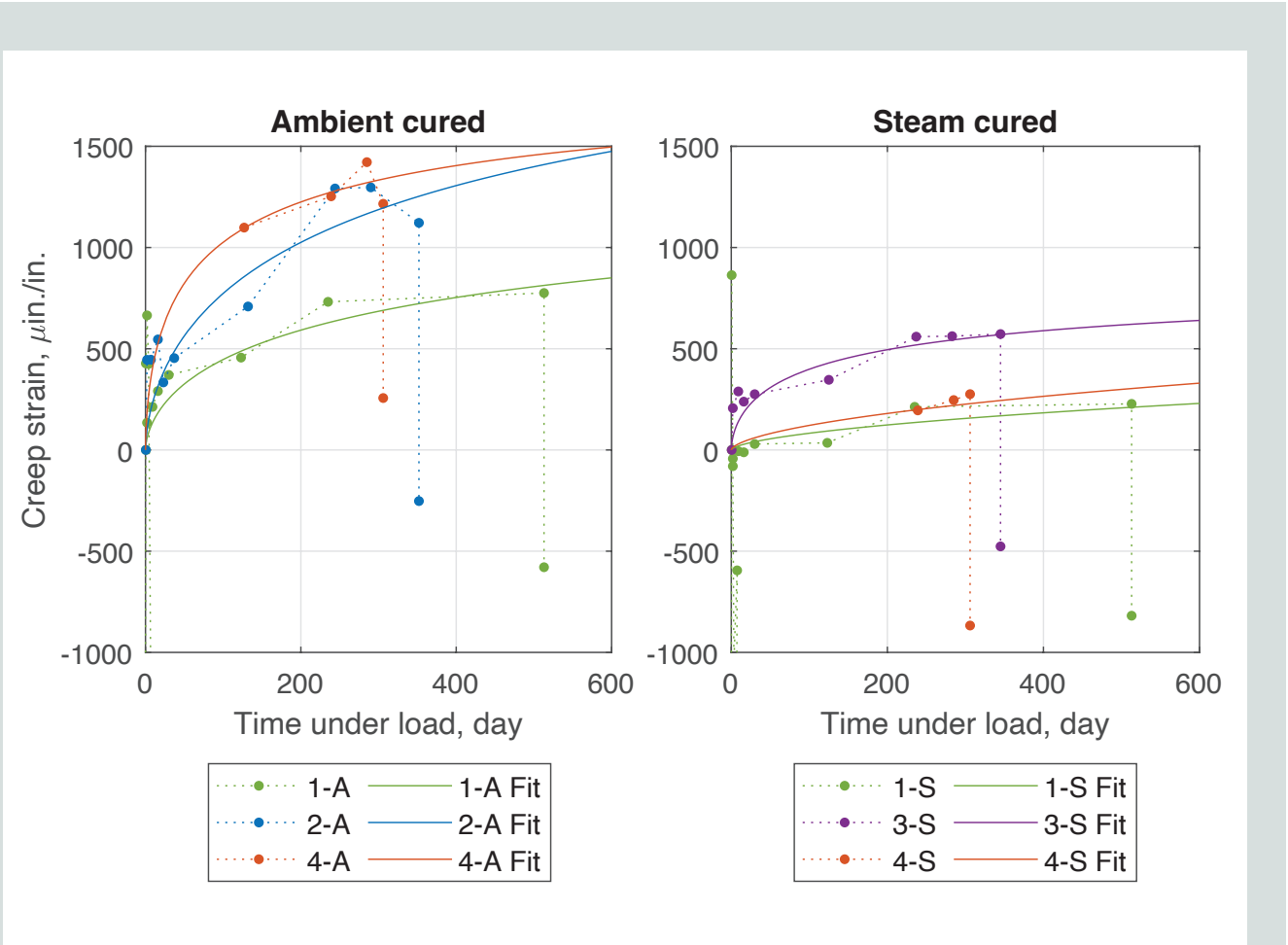

Figure 6. Creep strain for each ultra-high-performance concrete specimen. Note: Fit = trendline fit; 1-A = mixture proportions number 1 with ambient curing conditions; 1-S = mixture proportions number 1 with steam curing conditions; 2-A = mixture proportions number 2 with ambient curing conditions; 3-S = mixture proportions number 3 with steam curing conditions; 4-A = mixture proportions number 4 with ambient curing conditions; 4-S = mixture proportions number 4 with steam curing conditions.

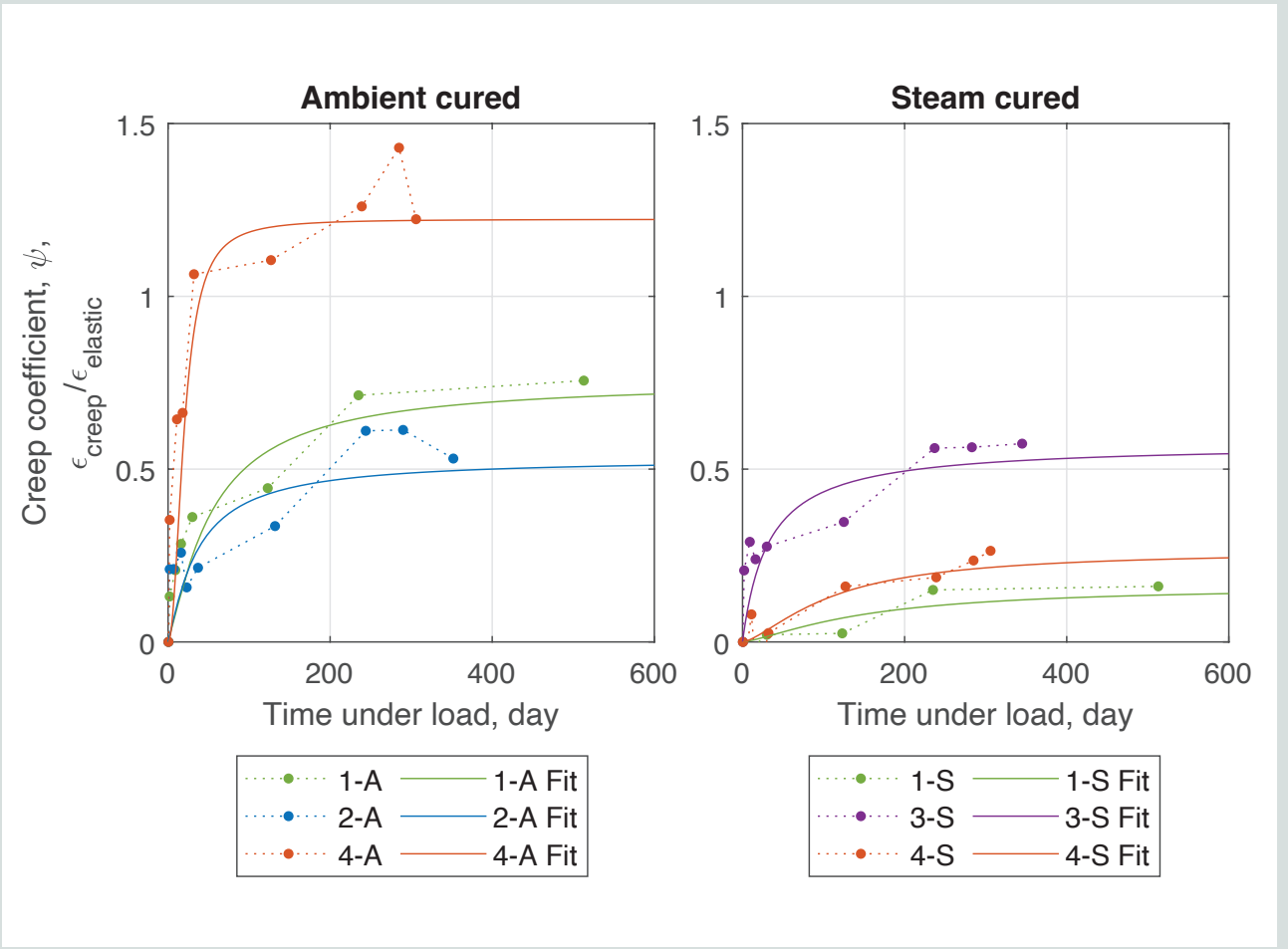

Figure 7. Creep coefficient calculated for each ultra-high-performance concrete specimen. Note: Fit = trendline fit; 1-A = mixture proportions number 1 with ambient curing conditions; 1-S = mixture proportions number 1 with steam curing conditions; 2-A = mixture proportions number 2 with ambient curing conditions; 3-S = mixture proportions number 3 with steam curing conditions; 4-A = mixture proportions number 4 with ambient curing conditions; 4-S = mixture proportions number 4 with steam curing conditions. ε_{creep} = creep strain; $\varepsilon_{elastic}$ = elastic strain.

In contrast, samples cured under steam conditions exhibited lower creep coefficients of approximately 0.10 to 0.50. Steam curing is well recognized as a means of accelerating the curing reactions;[44] the observed lower creep coefficients of the test specimens reflect the greater degree of hydration accomplished before creep loading. It is important to note that due to the test design, the applied load for each steam-cured specimen was a smaller proportion of the ultimate strength of the concrete, which also contributed to the reduction in creep coefficient.

It is also important to consider the age at which specimens are loaded; the degree of hydration of the material influences creep development. Because creep is caused by the loss of water in the capillary pores of the calcium silicate hydrate (CSH), a less-dense network of hydration products (such as in the ambient-cured specimens) implies that fewer CSH structures are available to distribute the creep load. The proportion of these capillary pores in UHPC is larger than in conventional concrete because UHPC has a greater cement content and lacks coarse aggregate. As a result, UHPC mixtures exhibit greater creep coefficients than conventional concrete. The high proportion of silica fume content and the addition of steel fibers in UHPC help mitigate these effects.[41] In addition, much of this strain (deformation) induced by creep phenomenon is recoverable or reversible due to UHPC's high strength and elasticity.[41]

For the experiments performed during this research, specimens from both curing conditions were loaded at the same age (7 days) to simulate the bed turnover in a precast concrete yard, regardless of the state of hydration. However, it is important to note that compared with the steam-cured specimens, the ambient-cured specimens had a lower degree of hydration (as evidenced by the lower compressive strength) and experienced significantly increased creep strains. For this reason, when ambient curing is to be used for industrial and practical applications, it may be preferable to permit a longer initial curing period to limit prestress losses due to creep.

Specific creep Specific creep is another method of quantifying creep effects, which considers the amount of com-

pressive load that is applied to the concrete. Creep coefficients for the investigated nonproprietary UHPC mixtures are summarized in **Table 4**. The table shows a trendline fit to the experimental creep strain; the trendlines were used to determine the predicted creep at 1 year. In addition, the table presents the predicted creep strain and specific creep at 1 year.

Specific creep was calculated by dividing the creep strain by the stress applied during loading (6 ksi [41.4 MPa]). The predicted creep at 1 year ranges from a minimum of 174 microstrain for 1-S specimens to 1360 microstrain for 3-A specimens. The predicted creep strain at 1 year is much greater for ambient-cured specimens than for steam-cured specimens, by as much as 200% to 500%. Since creep strain shares a proportional relationship with specific creep, the results for creep strain and specific creep are similar. Because specific creep is normalized by the applied stress, the greater strength of the UHPC and greater amount of applied prestress would lead to greater creep strains than those expected for conventional concretes.

Design impacts

This study evaluated how UHPC behavior compares to estimation models of creep and shrinkage intended for the design of conventional concrete. These comparisons were conducted to demonstrate to designers the relative magnitude of the experimental data as compared to currently used, well-known estimation models of prestress loss in precast elements. This information may be particularly helpful for designers who are not yet familiar with UHPC design or lack access to UHPC design guidelines.

Experimental creep and shrinkage strain estimates

Figures 8 and **9** present experimental shrinkage strains and experimental creep strains, respectively, for all test specimens with trendline fits. These figures also show plots of design estimation models for conventional concrete from the *PCI Design Handbook: Precast and Prestressed Concrete*.[46] Although the comparison is not perfect, ambient-cured experimental UHPC shrinkage data are paired with PCI design trendlines for moist-cured conventional concrete. Likewise, steam-cured experimental UHPC shrinkage data are paired with PCI design estimates for accelerated-cured conventional concrete. These comparisons were selected to approximate the "least effort required" and "more effort required" curing approaches a precaster may choose. **Table 5** summarizes the experimental trendline parameters.

Creep and shrinkage values were estimated at 1 year using the trendlines presented in Table 5. By 1 year, UHPC creep and shrinkage strains exceeded those estimated by design for conventional concrete. Ambient-cured UHPC exhibited greater strains than steam-cured UHPC, with ultimate predicted strains values of 1110 µin./in. for creep and 590 µin./in. for shrinkage. Under this curing regimen, the magnitude for creep registered was nearly five times that of conventional concrete, whereas the shrinkage magnitude only slightly exceeded that of conventional concrete. The *PCI Design Handbook* suggests that moist-cured conventional concrete is expected to exhibit 1-year creep strains of approximately 250 µin./in. and shrinkage strains of approximately 550 µin./in.

The applied steam-curing regimen (90°C ± 1.1°C and 100% relative humidity for 48 hours) had a drastic effect on both the observed creep and shrinkage strains for steam-cured specimens. Based on the experimental data, steam-cured

Table 4. Creep coefficient trendline

Specimen	Creep coefficient trendline				Strain trendline				
	$C(t) = t^{\psi}/(A + t^{\psi}) \times Cult$				$\varepsilon_{cr}(t) = t^{0.6}/(A \times t^{0.6}) \times B$				
	ψ	A	R^2	Predicted at 1 year	A	B	R^2	Predicted at 1 year, µin./in.	Predicted specific creep at 1 year, µin./in./ksi
1-A	1.21	124	0.926	0.69	40.8	1600	0.913	731	122
1-S	1.38	1000	0.816	0.12	559	3000	0.746	174	29
2-A	1.16	65	0.776	0.5	41.1	2780	0.856	1270	211
3-S	1	32	0.841	0.53	21.2	931	0.866	577	96
4-A	2.14	607	0.935	1.22	14.5	1960	0.848	1380	230
4-S	1.47	1000	0.745	0.22	376	3000	0.667	252	42

Note: Trendline forms as presented in Haber et al. (2019). 1-A = mixture proportions number 1 with ambient curing conditions; 1-S = mixture proportions number 1 with steam curing conditions; 2-A = mixture proportions number 2 with ambient curing conditions; 3-S = mixture proportions number 3 with steam curing conditions; 4-A = mixture proportions number 4 with ambient curing conditions; 4-S = mixture proportions number 4 with steam curing conditions. A = curve fit parameter; B = curve fit parameter; C_{ult} = creep coefficient immediately prior to unloading; R^2 = coefficient of determination; t = time under load in days ε_{cr} = creep strain; ψ = creep coefficient.

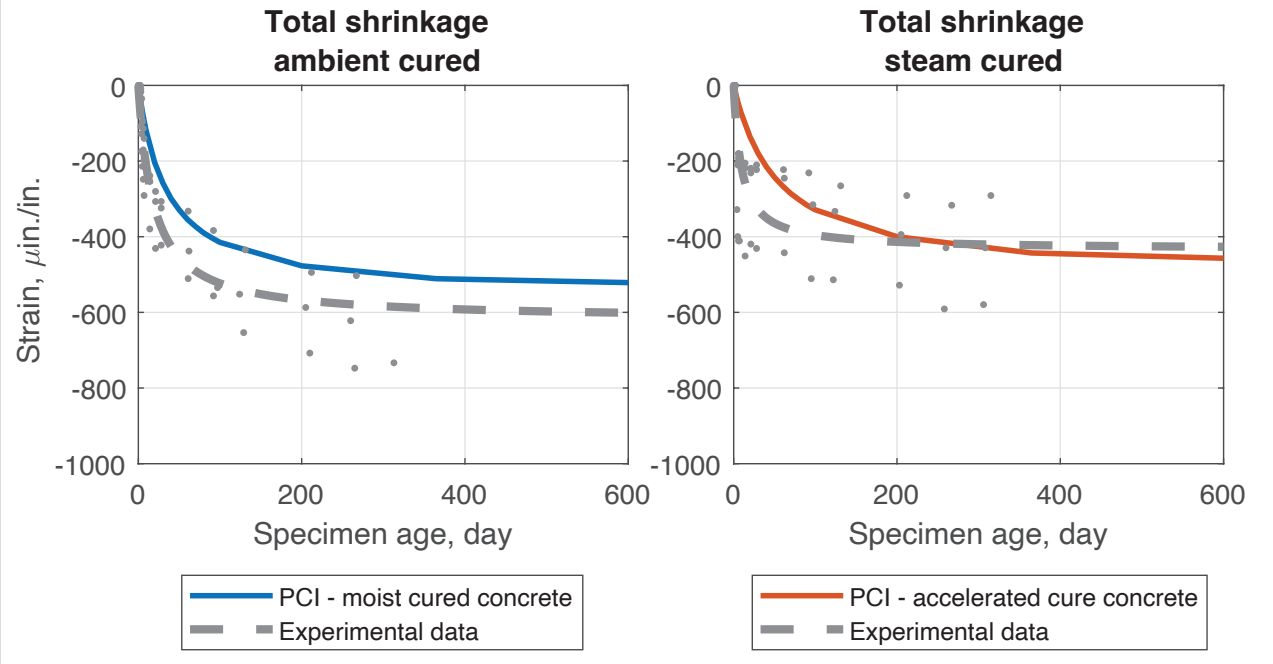

Figure 8. Shrinkage strains from all ultra-high-performance concrete specimens and predicted *PCI Design Handbook: Precast and Prestressed Concrete* model for conventional concrete.

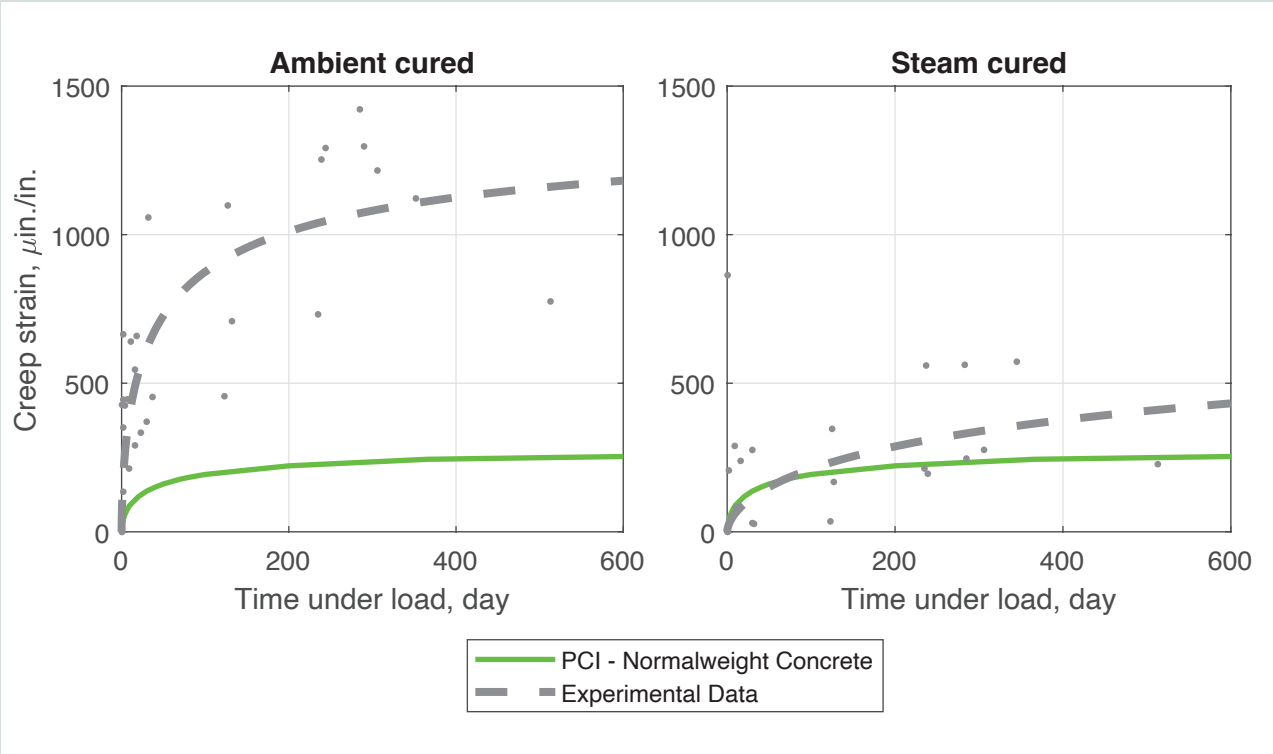

Figure 9. Creep strains from all ultra-high-performance concrete specimens and predicted *PCI Design Handbook: Precast and Prestressed Concrete* model for conventional concrete.

Table 5. Creep and shrinkage experimental strain trendline parameters

$\varepsilon_{sh}(t) = t/(A \times t) \times \varepsilon_{sh\text{-}ult}$		A	Average $\varepsilon_{sh\text{-}ult}$ (experimental)	R^2	Predicted strain at 1 year, ε_{sh} μin./in.
Shrinkage	Ambient cured	18.4	-611	0.884	-590
	Steam cured	9.5	-433	0.457	-422
$\varepsilon_{cr}(t) = t^{0.6}/(A \times t^{0.6}) \times B$		A	B	R^2	Predicted strain at 1 year, ε_{cr} μin./in.
Creep	Ambient cured	10.3	1440	0.717	1110
	Steam cured	54.7	942	0.468	364

Note: A = curve fit parameter; B = curve fit parameter; R^2 = coefficient of determination; t = time of measurement in days; ε_{cr} = predicted creep strain; ε_{sh} = predicted shrinkage strain; $\varepsilon_{sh\text{-}ult}$ = ultimate shrinkage strain.

UHPC was predicted to exhibit 1-year creep strains of about 364 μin./in. and shrinkage strains of 422 μin./in. The magnitude for creep for steam-cured UHPC was more than 100 μin./in. more than the magnitude predicted for accelerated-cured conventional concrete, but the shrinkage magnitude for steam-cured UHPC was lower than that of accelerated-cured conventional concrete. For the case of accelerated-cured conventional concrete, creep strain of approximately 250 μin./in. and shrinkage strain of 475 μin./in. are suggested design estimates.

When the long-term strain magnitudes demonstrated by steam-cured and ambient-cured UHPC were compared to those expected of conventional concrete, the authors found that magnitudes for the steam-cured specimens were the closest to the conventional concrete predictions. This assertion is particularly true for creep effects, where the estimated creep strain for ambient-cured UHPC was approximately five times greater than the creep strain recommended for conventional concrete. It is important to highlight the importance of the degree of hydration and age of loading when analyzing creep effects. In the experimental testing, ambient-cured and steam-cured samples were loaded at the same age and compressive stress to simulate bed turnover in a precast concrete facility. As a result, ambient-cured specimens had much lower degree of hydration than steam-cured specimens at the time of testing, as well as lesser strength and a subsequently greater load ratio. It is also important to note that the loads applied for both curing conditions were greater magnitude for UHPC than the ones used to evaluate conventional concrete samples. On the other hand, shrinkage strains for both curing regimens were close in magnitude to those for conventional concrete.

Table 5 shows that the coefficient of determination R^2 values for the trendlines modeled for ambient-cured specimens (0.884 for shrinkage and 0.717 for creep) are greater than the R^2 values exhibited for steam-cured specimens (0.457 for shrinkage and 0.468 for creep). These results indicate that the steam-cured strain data exhibited greater variability than that of the ambient-cured specimens; this finding is expected given that the steam-curing process accelerates and magnifies small differences in mixture design, particularly when the effects of chemical admixtures are considered. At early ages, a sharp increase in shrinkage strain in the steam-cured UHPC samples can be observed, resulting in a curve that does not follow the more gently sloped shape defined by the trendline. This effect was the result of the rapid increase in the degree of hydration instigated by the application of supplementary heat and moisture. A modification to the form of the trendline may be necessary to capture these effects. Additionally, errors in the creep data may also help explain why the R^2 values were lower for the steam-cured specimens. Some creep strain data points were negative following the subtraction of the initial elastic strain. These data points would indicate that the concrete relaxed under the initial elastic displacement and the creep model cannot easily account for them.

Creep coefficient for all experimental data **Figure 10** presents the results obtained for the calculation of creep coefficient for all the evaluated mixtures. A trendline was fit for the creep coefficient considering all mixture proportions and curing conditions. The results are presented in **Table 6**. Creep coefficients calculated for ambient-cured specimens ranged from 0.5 to 1.2 at the time of unloading. In contrast, the magnitude obtained for this parameter when evaluating steam-cured specimens ranged from 0.2 to 0.6 at the time of unloading, reflecting the greater degree of hydration and consequent greater compressive strength.

Table 6. Creep coefficient trendline

Curing condition	Creep coefficient trendline $C(t) = t^{\psi}/(A + t^{\psi}) \times C_{ult}$			
	ψ	A	C_{ult}	R^2
Ambient	0.438	9.33	1.52	0.473
Steam	0.738	48.6	0.551	0.592

Note: A = curve fit parameter C = curve fit parameter; C_{ult} = creep coefficient immediately prior to unloading; R^2 = coefficient of determination; t = time under load in days; ψ = creep coefficient.

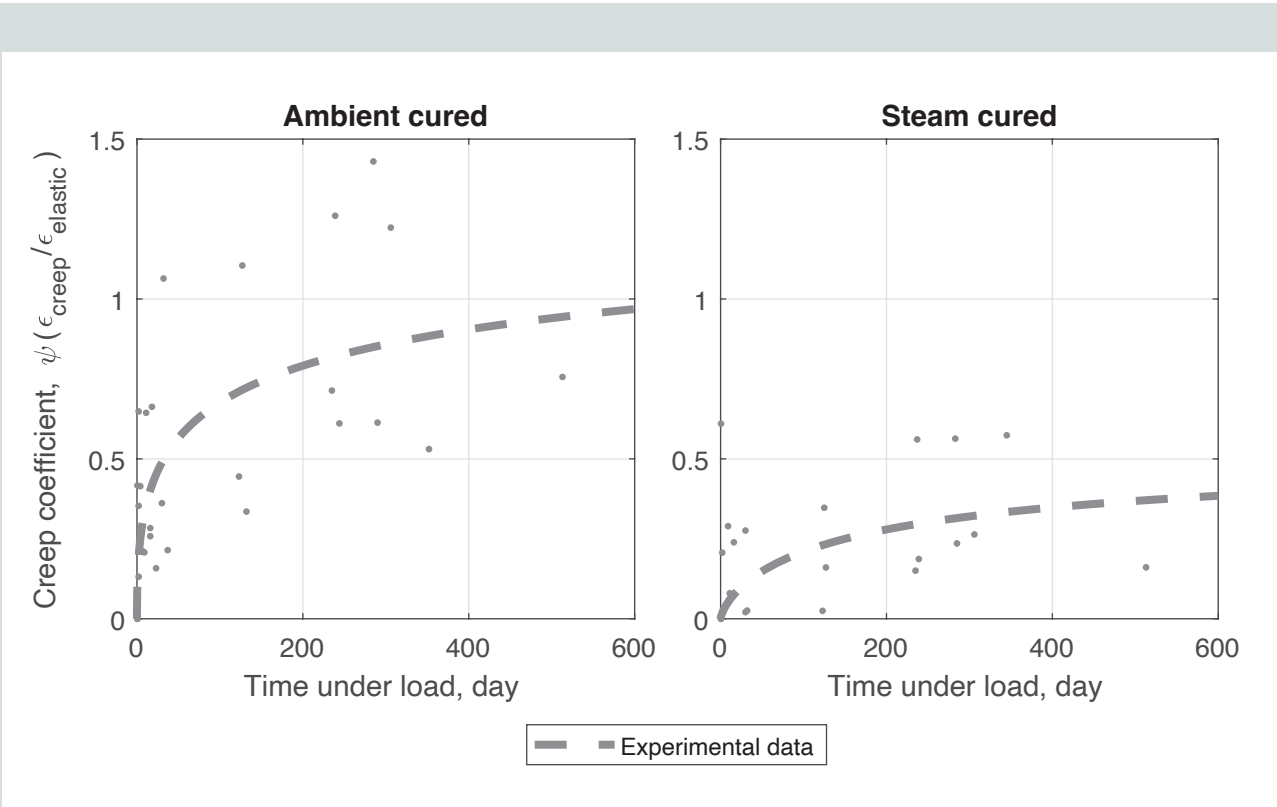

Figure 10. Creep coefficient data from all ultra-high-performance concrete.
Note: ε_{creep} = creep strain; $\varepsilon_{elastic}$ = elastic strain.

Conclusion and recommendations

Four nonproprietary UHPC mixture proportions developed by precasters in North America were employed to assess creep and shrinkage effects. Accepted test procedures were applied to characterize long-term material behavior. Although the study encountered difficulties during testing that were related to the nature of UHPC mixtures and the test methodologies, several conclusions can be drawn from the work:

- Curing of UHPC has a direct and immediate impact on time-dependent material properties. Curing regimens should be carefully considered in calculations of time-dependent prestress losses.
- Steam-cured specimens demonstrated greater compressive strength than ambient-cured specimens at 7 days (mean values of 20.8 and 15.4 ksi [143.4 and 106.2 MPa], respectively) and 28 days (mean values of 21.5 and 19.6 ksi [148.2 and 135.1 MPa], respectively).
- UHPC mixtures exhibited greater shrinkage strains than conventional concrete, especially when ambient-curing conditions are applied, with mean values for UHPC at 1 year of −590 µin./in. for ambient-cured specimens and -422 µin./in. for steam cured specimens.
- Drying shrinkage was observed to be relatively small (<150 µin./in.) and ambient-cured specimens exhibited greater values than steam-cured specimens, with mean values of 72 and 44 µin./in., respectively.
- UHPC mixtures exhibited greater creep strains than conventional concrete, especially when ambient-curing conditions were applied. The mean values for UHPC at 1 year were 1110 µin./in. for ambient-cured specimens and 364 µin./in. for steam cured specimens.
- Larger creep coefficients were obtained for ambient-cured UHPC specimens than for steam-cured UHPC specimens, with mean values at 1 year of 0.80 and 0.29, respectively.
- When UHPC strain values for ambient-cured and steam-cured specimens were compared to strain values of conventional concrete, the magnitudes for the steam-cured specimens were closer to the conventional concrete magnitudes, especially when comparing the results for creep.
- Steam-cured specimens exhibited more shrinkage strain than ambient-cured specimens during the testing period especially during early ages. This is attributable to increased hydration rates caused by the curing regime.

As industry applications of UHPC become more widely used, the development of a data bank of creep and shrinkage data specific to UHPC mixtures would be advisable to

account for the ways that the behaviors of UHPC mixtures differ from the behaviors of conventional concrete. Although UHPC mixtures demonstrate improved performance and properties compared with conventional concrete, UHPC tends to have larger ultimate creep and shrinkage strains, with corresponding effects on prestress losses. In addition, it is advisable to consider steam-curing regimens, whenever possible, to reduce the strains experienced by UHPC structural components. More research is needed to review and analyze the suggested prestress loss calculation methods for UHPC and to characterize the early-age shrinkage behavior of UHPC.

Acknowledgments

This research effort was funded by PCI. We greatly appreciate their support, as well as their patience while this research was conducted during the COVID-19 pandemic. We would also like to thank the many precasters, researchers, academics, and industry professionals who contributed their time, materials, and insight. Their contributions were invaluable to the project. Finally, we thank CTL for allowing us the use of their facilities.

References

1. Xue, J., B. Briseghella, F. Huang, C. Nuti, H. Tabatabai, and B. Chen. 2020. "Review of Ultra-High Performance Concrete and Its Application in Bridge Engineering." *Construction and Building Materials* 260: 119844. https://doi.org/10.1016/j.conbuildmat.2020.119844.

2. Amran, M., S. S. Huang, A. M. Onaizi, N. Makul, H. S. Abdelgader, and T. Ozbakkaloglu. 2022. "Recent Trends in Ultra-High Performance Concrete (UHPC): Current Status, Challenges, and Future Prospects." *Construction and Building Materials* 352: 129029. https://doi.org/10.1016/j.conbuildmat.2022.129029.

3. Russell, H. G., B. A. Graybeal, and H. G. Russell. 2013. *Ultra-High Performance Concrete: A State-of-the-Art Report for the Bridge Community*. FHWA-HRT-13-060. Washington, DC: Federal Highway Administration (FHWA). https://www.fhwa.dot.gov/publications/research/infrastructure/structures/hpc/13060.

4. Alsalman, A., C. N. Dang, and W. M. Hale. 2017. "Development of Ultra-High Performance Concrete with Locally Available Materials." *Construction and Building Materials* 133: 135–145. https://doi.org/10.1016/j.conbuildmat.2016.12.040.

5. Graybeal, B. A. 2013. *Development of Non-Proprietary Ultra-High Performance Concrete for Use in the Highway Bridge Sector*. FHWA-HRT-13-100. Washington, DC: FHWA. https://www.fhwa.dot.gov/publications/research/infrastructure/structures/bridge/13100/index.cfm.

6. El-Tawil, S., M. Alkaysi, A. E. Naaman, W. Hansen, and Z. Liu. 2016. *Development, Characterization and Applications of a Non Proprietary Ultra High Performance Concrete for Highway Bridges*. Ann Arbor: University of Michigan. https://rosap.ntl.bts.gov/view/dot/30887.

7. Abokifa, M., and M. A. Moustafa. 2021. "Mechanical Characterization and Material Variability Effects of Emerging Non-proprietary UHPC Mixes for Accelerated Bridge Construction Field Joints." *Construction and Building Materials* 308: 125064. https://doi.org/10.1016/j.conbuildmat.2021.125064.

8. Hasan, T. M., L. Gilbert, S. Allena, J. Owusu-Danquah, and A. Torres. 2022. "Development of Non-Proprietary Ultra-High Performance Concrete Mixtures." *Buildings* 12 (11): 1865. https://doi.org/10.3390/buildings12111865.

9. Shahrokhinasab, E., and D. Garber. 2021. *Development of "ABC-UTC Non-Proprietary UHPC" Mix*. Final Report. Miami: Florida International University Department of Civil Engineering. https://abc-utc.fiu.edu/wp-content/uploads/2021/05/ABC-UTC-2016-C2-FIU01-Final-Report_v2-1.pdf.

10. eConstruct USA LLC, Wiss, Janney, Elstner Associates Inc., University of Nebraska-Lincoln, and the NCSU Constructed Facilities Laboratory. 2020. *Implementation of Ultra-High-Performance Concrete in Long-Span Precast Pretensioned Elements for Concrete Buildings and Bridges*. Chicago, IL: PCI. https://doi.org/10.15554/pci.rr.mat-012.

11. Graybeal, B. A. 2006. *Material Property Characterization of Ultra-High Performance Concrete*. FHWA-HRT-06-103. Washington, DC: FHWA. https://highways.dot.gov/media/6141.

12. Shao, Y., and S. L. Billington. 2022. "Impact of UHPC Tensile Behavior on Steel Reinforced UHPC Flexural Behavior." *Journal of Structural Engineering* 148 (1): 04021244. https://doi.org/10.1061/(ASCE)ST.1943-541X.0003225.

13. Zhou, Z., and P. Qiao. 2019. "Tensile Behavior of Ultra-High Performance Concrete: Analytical Model and Experimental Validation." *Construction and Building Materials* 201: 842–851. https://doi.org/10.1016/j.conbuildmat.2018.12.137.

14. Pansuk, W., H. Sato, Y. Sato, and R. Shionaga. 2008. "Tensile Behaviors and Fiber Orientation of UHPC." In *Proceedings of the Second International Symposium on Ultra High Performance Concrete, Kassel, Germany, 5–7 March 2008*, edited by E Fehling, M. Schmidt, and S. Stürwald, 161–168. Kassel, Germany: Kassel University Press.

15. Graybeal, B. 2015. "Tensile Mechanical Response of Ultra-High-Performance Concrete." *Advances in Civil Engineering Materials* 4 (2): 62–74. https://doi.org/10.1520/ACEM20140029.

16. Graybeal, B., and M. Davis. 2008. "Cylinder or Cube: Strength Testing of 80 to 200 MPa (11.6 to 29 ksi) Ultra-High-Performance Fiber-Reinforced Concrete." *ACI Materials Journal* 105 (6): 603–609. https://doi.org/10.14359/20202.

17. Naeimi, N., and M. A. Moustafa. 2021. "Compressive Behavior and Stress–Strain Relationships of Confined and Unconfined UHPC." *Construction and Building Materials* 272: 121844. https://doi.org/10.1016/j.conbuildmat.2020.121844.

18. Graybeal, B. A. 2007. "Compressive Behavior of Ultra-High-Performance Fiber-Reinforced Concrete." *ACI Materials Journal* 104 (2): 146–152. https://doi.org/10.14359/18577.

19. Graybeal, B., and J. Tanesi. 2007. "Durability of an Ultra High-Performance Concrete." *Journal of Materials in Civil Engineering* 19 (10): 848–854. https://doi.org/10.1061/(ASCE)0899-1561(2007)19:10(848).

20. Li, J., Z. Wu, C. Shi, Q. Yuan, and Z. Zhang. 2020. "Durability of Ultra-High Performance Concrete–A Review." *Construction and Building Materials* 255: 119296. https://doi.org/10.1016/j.conbuildmat.2020.119296.

21. Abbas, S., M. Nehdi, and M. Saleem. 2016. "Ultra-High Performance Concrete: Mechanical Performance, Durability, Sustainability and Implementation Challenges." *International Journal of Concrete Structures and Materials* 10: 271–295. https://doi.org/10.1007/s40069-016-0157-4.

22. Mohebbi, A., B. Graybeal, and Z. Haber. 2022. "Time-Dependent Properties of Ultrahigh-Performance Concrete: Compressive Creep and Shrinkage." *Journal of Materials in Civil Engineering* 34 (6): 04022096. https://doi.org/10.1061/(ASCE)MT.1943-5533.0004219.

23. Mohebbi, A., Z. Haber, and B. A. Graybeal. 2019. "Evaluation of AASHTO Provisions for Creep and Shrinkage of Prestressed UHPC Girders." *International Interactive Symposium on Ultra-High Performance Concrete* 2 (1). https://doi.org/10.21838/uhpc.9706.

24. American Concrete Institute (ACI). 2008. *Prediction of Creep, Shrinkage, and Temperature Effects in Concrete Structures (Reapproved 2008).* ACI PRC-209-92. Farmington Hills, MI: ACI.

25. ASTM International.2019. *Standard Test Method for Total Evaporable Moisture Content of Aggregate by Drying*. ASTM C566-19. West Conshohocken, PA: ASTM International.

26. ASTM International. 2020. *Standard Test Method for Flow of Hydraulic Cement Mortar*. ASTM C1437-20. West Conshohocken, PA: ASTM International.

27. ASTM International. 2017. *Standard Practice for Fabricating and Testing Specimens of Ultra-High Performance Concrete*. ASTM C1856/C1856M-17. West Conshohocken, PA: ASTM International.

28. ASTM International. 2017. *Standard Test Method for Length Change of Hardened Hydraulic-Cement Mortar and Concrete*. ASTM C157/C157M-17. West Conshohocken, PA: ASTM International.

29. ASTM International.2019. *Standard Test Methods for Time of Setting of Hydraulic Cement by Vicat Needle*. ASTM C191-19. West Conshohocken, PA: ASTM International.

30. Yalçınkaya, Ç., and H. Yazıcı. 2017. "Effects of Ambient Temperature and Relative Humidity on Early-age Shrinkage of UHPC with High-Volume Mineral Admixtures." *Construction and Building Materials* 2017; 144: 252–259. https://doi.org/10.1016/j.conbuildmat.2017.03.198.

31. ASTM International.2019. *Standard Test Method for Autogenous Strain of Cement Paste and Mortar*. ASTM C1698-19. West Conshohocken, PA: ASTM International.

32. ASTM International.2015. *Standard Test Method for Creep of Concrete in Compression*. ASTM C512-15/C512-15M. West Conshohocken, PA: ASTM International.

33. ACI. 2019. *Building Code Requirements for Structural Concrete: (ACI 318-19) and Commentary (ACI 318R-19).* Farmington Hills, MI: ACI.

34. ASTM International.2020. *Standard Test Method for Compressive Strength of Cylindrical Concrete Specimens*. ASTM C39/C39M-20. West Conshohocken, PA: ASTM International.

35. ASTM International. 2014. *Standard Test Method for Static Modulus of Elasticity and Poisson's Ratio of Concrete in Compression*. ASTM C469/C469M-14. West Conshohocken, PA: ASTM International.

36. Yoo, D. Y., S. Kim, and M. J. Kim. 2018. "Comparative Shrinkage Behavior of Ultra-High-Performance Fiber-Reinforced Concrete under Ambient and Heat Curing Conditions." *Construction and Building Materials* 162: 406–419. https://doi.org/10.1016/j.conbuildmat.2017.12.029.

37. Mehta, P., and P. J. M. Monteiro. 2005. *Concrete : Microstructure, Properties, and Materials: Microstructure, Properties, and Materials*. 3rd ed. New York, NY: McGraw-Hill.

38. Zhang, M. H., C. T. Tam, and M. P. Leow. 2003. "Effect of Water-to-Cementitious Materials Ratio and Silica Fume on the Autogenous Shrinkage of Concrete." *Cement and Concrete Research* 33 (10): 1687–1694. https://doi.org/10.1016/S0008-8846(03)00149-2.

39. Tam, V. W., D. Kotrayothar, and J. Xiao. 2015. "Long-Term Deformation Behaviour of Recycled Aggregate Concrete." *Construction and Building Materials* 100: 262–272. https://doi.org/10.1016/j.conbuildmat.2015.10.013.

40. Weiss J. 2003. "Experimental Determination of the 'Time Zero', t0 ('Maturity-Zero', M0)." In *Early Age Cracking in Cementitious Systems—Report of RILEM Technical Committee 181-EAS—Early Age Shrinkage Induced Stresses and Cracking in Cementitious Systems*, edited by A. Bentur, 195–206. Champs-sur-Marne, France: RILEM Publications. https://doi.org/10.1617/2912143632.019.

41. Bentur, A. 2003. "Terminology and Definitions." 2003. In *Early Age Cracking in Cementitious Systems—Report of RILEM Technical Committee 181-EAS—Early Age Shrinkage Induced Stresses and Cracking in Cementitious Systems*, edited by A. Bentur, 13–15. https://doi.org/10.1617/2912143632.002.

42. AASHTO (American Association of State Highway and Transportation Officials). 2000. *Standard Method of Test for Time of Setting of Concrete mixtures by Penetration Resistance*. AASHTO T197M/T 197. Washington, DC: AASHTO.

43. Wang, D., C. Shi, Z. Wu, J. Xiao, Z. Huang, and Z. Fang. 2015. "A Review on Ultra High Performance Concrete: Part II. Hydration, Microstructure and Properties." *Construction and Building Materials* 96: 368–377. https://doi.org/10.1016/j.conbuildmat.2015.08.095.

44. Chern, J., and C. Chang. 1994. "Effects of Silica Fume on Creep and Shrinkage of Steel Fiber Reinforced Concrete." *ACI Symposium Papers* 149: 561–574. https://doi.org/10.14359/4098.

45. Haber, Z. B., I. De la Varga, B. A. Graybeal, B. Nakashoji, and R. El-Helou. 2018. Properties and behavior of UHPC-class materials. Washington, DC: U.S Federal Highway Administration Office of Infrastructure.

46. PCI. 2017. *PCI Design Handbook: Precast and Prestressed Concrete*. 8th ed. Chicago, IL: PCI.

Notation

A = curve fit parameter

B = curve fit parameter

$C(t)$ = predicted creep coefficient as a function of time in days

C_{ult} = creep coefficient immediately prior to unloading

f'_{ci} = concrete compressive strength

R^2 = coefficient of determination

t = time in days

ε_{creep} = creep strain

$\varepsilon_{elastic}$ = elastic strain

ε_{sh} = shrinkage strain

$\varepsilon_{sh\text{-}ult}$ = ultimate shrinkage strain

ε_{ult} = ultimate total strain

ε_{cr} = creep strain

ψ = creep coefficient

About the authors

Garrett Tatum is a PhD candidate in the Department of Civil, Environmental, and Geodetic Engineering at The Ohio State University in Columbus. His research interests are in the durability of wood and concrete structures. His experimental and computational efforts seek to quantify how microstructural changes affect structural components. He has been supported by a National Science Foundation Graduate Research Fellowship.

Lautaro Martinez is a civil engineer. He graduated from the National Technological University of Argentina and is currently pursuing a master of science degree in the Department of Civil, Environmental, and Geodetic Engineering at The Ohio State University. His research interests are mainly focused on the performance of concrete and timber structures and natural hazards in structural engineering. He has been supported by a Fulbright Scholarship.

Natassia Brenkus, PhD, is an assistant professor at The Ohio State University. Her research focus has been structural performance and durability of concrete bridge systems, with particular specialization in post-tensioning. Her recent research has been funded by PCI, the American Concrete Institute, and the Ohio Department of Transportation. She has more than a decade of experience investigating innovative bridge technologies and new construction techniques to advance the state-of-the-art of concrete bridges, and she is always looking forward to the next project.

Abstract

This paper presents the results of the experimental evaluation of four nonproprietary ultra-high-performance concrete (UHPC) mixture proportions currently being used for industrial applications by various precast concrete producers across the United States and Canada. The main objective of this research was to acquire data about the effects that creep and shrinkage phenomena produced with UHPC materials. Shrinkage was assessed by the ASTM C157 testing method modified by ASTM C1865 and ASTM C1698. Creep was evaluated by the ASTM C512 testing method modified by ASTM C1856. Results for creep and shrinkage strains and creep coefficient are presented and discussed. Comparisons with conventional concrete are also made. This detailed characterization of creep and shrinkage properties of the nonproprietary UHPC mixture proportions advances the understanding of UHPC materials and phenomena and offers useful information for further research on applications of UHPC for prestressed concrete structural components.

Keywords

Creep, prestressed concrete, shrinkage, UHPC, ultra-high-performance concrete.

Review policy

This paper was reviewed in accordance with the Precast/Prestressed Concrete Institute's peer-review process. The Precast/Prestressed Concrete Institute is not responsible for statements made by authors of papers in *PCI Journal*. No payment is offered.

Publishing details

This paper appears in *PCI Journal* (ISSN 0887-9672) V. 69, No. 5, September–October 2024, and can be found at https://doi.org/10.15554/pcij69.5-02. *PCI Journal* is published bimonthly by the Precast/Prestressed Concrete Institute, 8770 W. Bryn Mawr Ave., Suite 1150, Chicago, IL 60631.

Reader comments

Please address any reader comments to *PCI Journal* editor-in-chief Tom Klemens at tklemens@pci.org or Precast/Prestressed Concrete Institute, c/o *PCI Journal*, 8770 W. Bryn Mawr Ave., Suite 1150, Chicago, IL 60631.